Journal of Industrial and Engineering Chemistry 75 (2019) 138–147

Contents lists available at ScienceDirect

Journal of Industrial and Engineering Chemistry

journal homepage: www.elsevier.com/locate/jiec

Design and synthesis of acceptor–donor–acceptor small molecule based on caffeine derivative for efficient and stable polymer solar cells

Ye Jin Lee, Sung Jae Jeon, Jun Young Choi, Doo Kyung Moon*

Nano and Information Materials (NIMs) Laboratory, Department of Chemistry Engineering, Konkuk University, 120, Neungdong-ro, Gwangjin-gu, Seoul 05029, Republic of Korea

ARTICLE INFO

Article history:
Received 15 October 2018
Received in revised form 8 February 2019
Accepted 9 March 2019
Available online 15 March 2019

Keywords:
Caffeine
Non-covalent interaction
Polymer solar cell
Stability

ABSTRACT

We designed and synthesized IDTBTCf (Indacenodithiophene-benzothiadiazolecaffeine) non-fullerene acceptor by using the caffeine derivative as the electron withdrawing end-group. It showed strong polarization that is possible to improve stability by causing non-covalent interaction in active layer. When 2.5 wt% IDTBTCf was introduced as the third component in PTB7:$PC_{71}BM$ binary blend, the power conversion efficiency (PCE) is more higher value of 8.7% than the reference (8.4%). As a result of stability measurement without encapsulation in a glove box for 172 h, a device with IDTBTCf (degradation rate of efficiency, 8%) showed better stability than the reference one (degradation rate of efficiency, 15.5%).

Introduction

Polymer solar cells (PSCs) have attracted much attention as 'next-generation solar cell' due to their diverse advantages such as flexibility, light weight, and potential to develop reasonable and cost-effective process using the solution based process [1–3]. In order to obtain high efficiency PSCs, the power conversion efficiency (PCE) is achieved over 13% due to many studies which are the development of donor and acceptor materials [4–8], and device optimization [9–12], and others [5,13–17]. In spite of such efforts, there still remain challenges for commercialization of PSCs that need to be solved to overcome their short lifetime [18,19].

In general, fullerene derivatives, which have compatibility with various donors and potential to commercialization, are mainly used as acceptors of PSCs. However, there have been the problems of fullerene acceptor such as restricted visible light absorption region, limit of open circuit voltage (V_{OC}), high production cost, low stability and so on [20–23]. According to a recent study, a fullerene derivative makes self-aggregation over time in the active layer and decreases device stability [24]. Therefore, developing and applying new materials are necessary to maintain long-term stability by overcoming the disadvantages of the fullerene.

The strategies inducing intermolecular non-covalent interaction have been recently reported to improve stability of PSCs. Zhao et al. reported small molecule acceptors 'ITIC-Th1' where a fluorine atom was incorporated onto the end-capping group of 1,1-dicyanomethylene-3-indanone (IC). The incorporation of the fluorine atom enhanced electron mobility by inducing C—F···S, C—F···H, and C—F···π non-covalent interactions. As a result, a device achieved high PCE by enhancing short circuit current density (J_{SC}) and fill factor (FF) and showed excellent stability [25]. Cheng et al. reported their results that have improved device performance and stability by adding 4,4′-biphenol (BPO) in the active layer. Adding BPO made it possible to molecular locking structure by creating non-covalent interaction between fluorine-containing donor and fullerene acceptor blend. As a result, better stability was obtained by enhancing of π–π stacking in active layer [26].

In this study, we introduced caffeine (1,3,7-trimethylpurine-2,6-dione) into PSCs to improve stability. Because caffeine has two amide groups with strong negative potential, it easily able to induce inter-/intramolecular non-covalent interactions. To verify such effect, we developed the caffeine-based A–D–A type small molecule,Indacenodithiophene-benzothiadiazolecaffeine (IDTBTCf) and applied them to PSCs. IDTBTCf is composed of benzothiadiazolecaffeine (BTCf), which introduced benzothiadiazole to compensate for poor electron affinity of caffeine, as A unit and indacenodithiophene (IDT) which has excellent mobility and coplanar characteristics, as D unit [27].

We confirmed that the strong polarization occurred in the IDTBTCf by calculating of electrostatic potential (ESP) through the Gaussian. It suggesting that stability can be improved via non-covalent interaction between donor and acceptor when introduced in the active layer. Indeed, when 2.5 wt% IDTBTCf was introduced as the third component in PTB7:$PC_{71}BM$ binary blend and the

* Corresponding author.
E-mail address: dkmoon@konkuk.ac.kr (D.K. Moon).

https://doi.org/10.1016/j.jiec.2019.03.015
1226-086X/

device was manufactured with an inverted structure, it resulted in a slightly higher PCE of 8.7% than the reference PCE of 8.4%. As a result of long-term stability measurement without encapsulation in a glove box for 172 h, a device with IDTBTCf (degradation rate of efficiency, 8%) showed better stability than the reference one (degradation rate of efficiency, 15.5%).

Experimental section

Theoretical simulation

Geometries and electron densities of states of the molecules were simulated through DFT calculation. To minimize computational time, calculation was performed by simplifying long alkyl chain of IDT into methyl groups. The lowest unoccupied molecular orbitals (LUMO) energy levels of caffeine and its derivatives (thiophene-caffeine: T-Cf, benzothiadiazole-caffeine: BT-Cf) are showed in Fig. 1(a). To compensate for the low electron affinity of caffeine as an acceptor unit, its electron withdrawing characteristic was attempted to improve by flanking caffeine with the thiophene and benzothiadiazole, respectively. As the results of calculation, LUMO energy levels of caffeine derivatives were −1.649 eV of T-Cf and −2.820 eV of BT-Cf, respectively, which is lower than −0.819 eV of caffeine. It implies that lower band gap materials of A–D–A type can be synthesized if caffeine is connected with the much stronger electron deficient molecules. When compared with T-Cf and BT-Cf, electron clouds are delocalized from caffeine towards more electron deficient molecules.

Optimal geometries with the highest occupied molecular orbitals (HOMO) and LUMO energy levels of IDTBTCf are depicted through DFT calculations in Fig. 1(b). The HOMO and LUMO energy levels of IDTBTCf were −5.211 eV and −3.051 eV, respectively.

The electrostatic potential (ESP) image of IDTBTCf where polar caffeine groups were introduced at both ends is depicted in

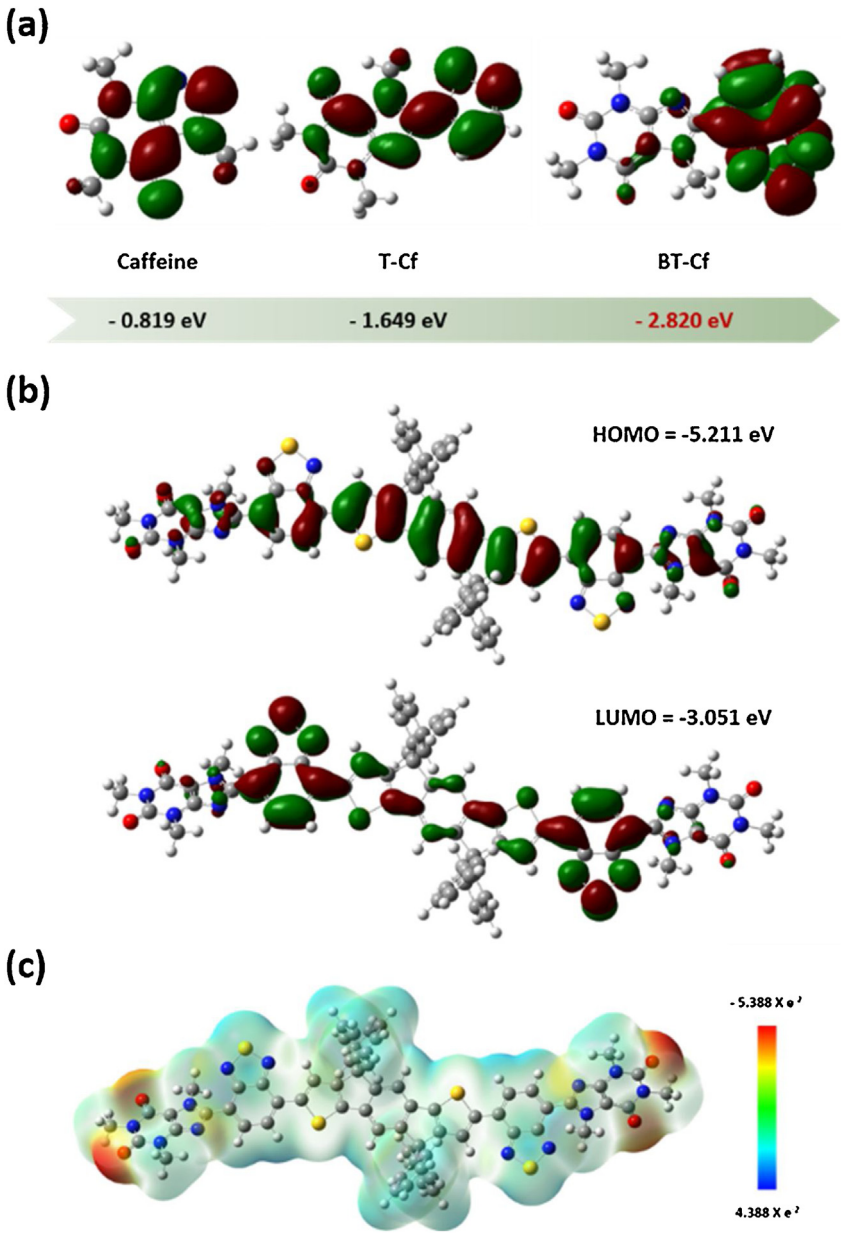

Fig. 1. (a) DFT calculation of the caffeine, T-Cf and BT-Cf moieties with LUMO, (b) DFT calculation of IDTBTCf with HOMO and LUMO, (c) ESP image of IDTBTCf.

Fig. 1(c). The chemical structure of caffeine, an electron shift direction by electronegativity differences, and the results of ESP calculation were shown in Fig. S1(a–c). As seen in Fig. S1(b), because electronegativity differences between carbon–oxygen and carbon–nitrogen single covalent bonds at the terminal positions of caffeine cannot be offset, strong polarization occurred in the IDTBTCf structure as in Fig. 1(c) [28].

Thus, when IDTBTCf is added to PTB7:$PC_{71}BM$ blend as the third material, new intermolecular non-covalent interactions such as hydrogen bonding and Van der Waals forces can be formed with donor and acceptor in the active layer. It can be expected to enhance performance and device stability [25].

Materials

The synthetic routes of IDTBTCf is depicted in Scheme 1. BT-Cf (3) was synthesized by direct arylation coupling reaction according to a previous reported procedure [29]. IDTBTCf was synthesized via stille coupling reaction with both synthesized BT-Cf (3) and IDT (4) under vial-assisted microwave irradiation [30]. (1), (2), catalysts, reagents and solvents were purchased from Aldrich. IDT (4) was purchased from Sunatech Inc. Chemicals were used without further purification. All products were purified by column chromatography using silica gel (230–400, Merck) as a stationary phase.

Synthesis of 8-(benzo[c][1,2,5]thiadiazol-4-yl)-1,3,7-trimethyl-1H-purine-2,6(3H,7H)-dione (BT-Cf) (3)

1 (Caffeine, 680 mg, 3.4 mmol), 2 (1 g, 3.4 mmol), Pivalic acid (102 mg, 1.02 mmol), K_2CO_3 (1.64 g, 11.9 mmol), $Pd_2(dba)_3$ (153 mg, 170 μmol) and P(o-tol)$_3$ (153 mg, 510 μmol) were added in 50 ml Schlenk-Flask flushed with nitrogen gas. After adding 17 ml of Dimethylformamide (DMF), the reaction mixture was refluxed for 24 h at 100 °C. After cooling to the room temperature, the reaction mixture was completely dissolved with chloroform. Then, the solution was extracted and the remained organic layer was dried. 3 (BT-Cf) 0.6 g (1.48 mmol, 44%) was obtained as yellow solid by column chromatography (Ethyl acetate, E.A:Hexane = 7:3). ^{1}H NMR (400 MHz, $CDCl_3$): δ 8.021–8.041 (d, 1H), 7.819–7.831 (d, 1H), 3.961 (s, 3H), 3.644 (s, 3H), 3.469 (s, 3H).

Synthesis of 8,8′-(7,7′-(thieno[3,2-b]thiophene-2,5-diyl)bis(4,4,9,9-tetrakis(4-hexylphenyl)-4,9-dihydro-s-indaceno[1,2-b:5,6-b′]dithiophene-2,7-diyl))bis(1,3,7-trimethyl-1H-purine-2,6(3H,7H)-dione) (IDTBTCf)

In a 2–5 ml microwave vial, 4 (186 mg, 0.15 mmol), 3 (BT-Cf, 146.6 mg, 0.36 mmol), $Pd_2(dba)_3$ (2.65 mg, 2.39 μmol) and P(o-tol)$_3$ (3.76 mg, 1.13 μmol) were added, and the mixture was dissolved in chlorobenzene (CB) 2.5 ml. The vial was vacuumed for 10 min and purged with nitrogen gas. The reactions were performed step-wisely at 100 °C for 5 min, 140 °C for 5 min, and 160 °C for 30 min, respectively, in the microwave reactor. After cooling to the room temperature, the reaction mixture was extracted with chloroform and dried. After being purified by flash column chromatography (E.A: Hexane = 4:6), the solid was recrystallized with ethanol to obtain 161 mg of IDTBTCf (0.103 mmol, 68%) as magenta solid. ^{1}H NMR (400 MHz, $CDCl_3$): δ 8.168 (s, 1H), 7.967–7.986 (d, 1H), 7.915–7.934 (d, 1H), 7.261–7.279 (d, 1H), 7.110–7.131 (d, 1H), 3.962 (s, 3H), 3.658 (s, 3H), 3.472 (s, 3H), 2.562–2.601 (m, 4H), 1.260–1.360 (m, 14 H), 0.850–0.883 (m, 8H). Elemental analysis (EA), found (%): C, 70.49; H, 5.82; N, 10.55; S, 12.07; O, 3.23.

Instruments

^{1}H NMR spectra were measured using the Bruker ARX 400 spectrometer in diluting the material into $CDCl_3$. The chemical concentration was detected based on the TMS added in ppm units as a standard material. Elemental analysis (EA) was performed using a Thermofinnigan EA2000. Thermogravimetric analysis (TGA) was measured using an NETZSCH TG 209 F3 thermogravimetric analyzer under the condition of nitrogen gas. The density functional theory (DFT) calculation used hybrid B3LYP correlation functional, and the split valence 6–31 G(d) basis set as implemented in the Gaussian 09 suite of programs. Absorption spectra were measured using an HP Agilent 8453 UV–vis spectrophotometer after diluting a single-component in chloroform and a blend in CB containing trace amounts of 1,8-diiodooctane (DIO). Cyclic voltammetry waves used Zahner IM6eX electrochemical workstation and 0.1 M acetonitrile solution replaced by nitrogen was used. Tetrabutylammonium hexafluorophosphate (Bu_4NPF_6) was used as an electrolyte. The constant scan rate was 50 mV s^{-1} and ITO, a Pt plate, silver/silver chloride [Ag in 0.1 M KCl] were used as working, counter, reference

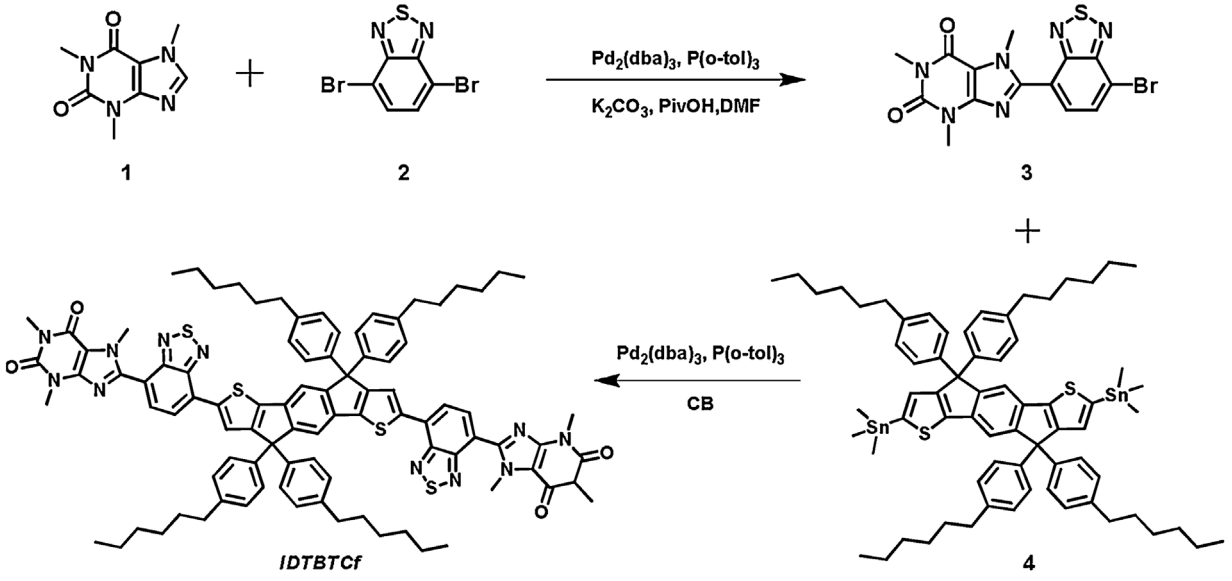

Scheme 1. Synthesis routes of IDTBTCf.

electrodes, respectively. Electrochemical potential was calibrated with half-wave potential of Fc/Fc^{+}. Photoluminescence (PL) spectra were measured in chloroform using an HP Agilent 8453 UV–vis spectrophotometer and Perkin Elmer LS55. XRD patterns were obtained using a Smart Lab 3 kW (40 kV 30 mA, Cu target, wavelength: 1.541871 Å) instrument of Rigaku, Japan. Topographic images of the active layers were obtained through atomic force microscopy (AFM) in a tapping mode under ambient conditions using a Multimode 8 instrument. Short current density–voltage (J–V) characteristics were measured by Keithley 2400 source meter unit. The light source used the solar simulator (Oriel, 1000 W) and reference cell was calibrated under AM 1.5 G under 100 mW/cm^2. And external quantum efficiency (EQE) characteristics were measured by Polaronix K3100 IPCE measurement system (Mc science). The contact angles of active layer materials were measured using DSA100 (KRUSS) instrument.

Results and discussion

Characterization

IDTBTCf was well dissolved in common solvents such as tetrahydrofuran (THF), chloroform ($CHCl_3$), and CB. In addition, the synthesized chemical structures were confirmed by EA and ^{1}H NMR (Figs. S2 and S3). As the result of TGA under the nitrogen gas, IDTBTCf showed an excellent thermal stability property, 5 wt% loss at 433.8 °C (Fig. S4).

Optical and electrochemical properties

Chemical structures of materials used in active layer are shown in Fig. 2(a). Fig. 2(b) shows the normalized UV–vis absorption spectra of IDTBTCf in chloroform solution and thin film states. IDTBTCf shows absorption peak for π–π^* transitions at 300–400 nm in the short wavelength region and strong intramolecular charge transfer (ICT) interaction between IDT and BT-Cf at 400–650 nm in the long wavelength region [31,32]. It is confirmed that UV absorption was broadly expanded from in solution state (450–600 nm) to form in film state (400–650 nm), and maximum absorption peak (λ_{max}) was red-shifted from 555 nm to 559 nm. This tendency is a result of high aggregation and packing between molecules in thin film [33]. In addition, the average extinction coefficient at maximum absorption peak was calculated based on the Bragg's law and the data of UV spectra in solutions of four different concentrations as seen in Fig. S5. As a result, the extinction coefficient (ε_{max} at 555 nm) of IDTBTCf was 70,203 M^{-1} cm^{-1}. It is slightly low as small molecule acceptor, but we can expect a compensation for the lack of optical absorption region in PTB7 and $PC_{71}BM$ blend at 450–600 nm by adding IDTBTCf as third component which is beneficial to capture more solar photons [34]. The optical band gap of IDTBTCf was calculated as 1.94 eV (λ_{onset} = 640 nm) in thin film state. It is expected that IDTBTCf forms adequate energy band gap between PTB7 and $PC_{71}BM$ energy levels. Thus, it will promotes charge carrier transfer in active layer.

The UV–vis spectra of the films used for the active layer materials are shown in Fig. 2(c). PTB7 and $PC_{71}BM$ showed UV absorption ranges of 600–750 nm and 300–600 nm, respectively. The synthesized IDTBTCf showed a new absorption range of 400–650 nm where donor and acceptor cannot be absorbed. Therefore, it is suitable to apply as the third component due to optical complementary absorption with donor and acceptor materials [16,35].

As shown in Fig. S6, cyclic voltammograms (CV) were measured to investigate whether IDTBTCf can have energy levels alignment between PTB7 and $PC_{71}BM$. The HOMO energy level of IDTBTCf was calculated as −5.44 eV by an electrochemical equation {E_{HOMO} (eV) = − 4.8 − (E_{onset} − $E_{1/2}$(Ferrocene)} where ferrocene

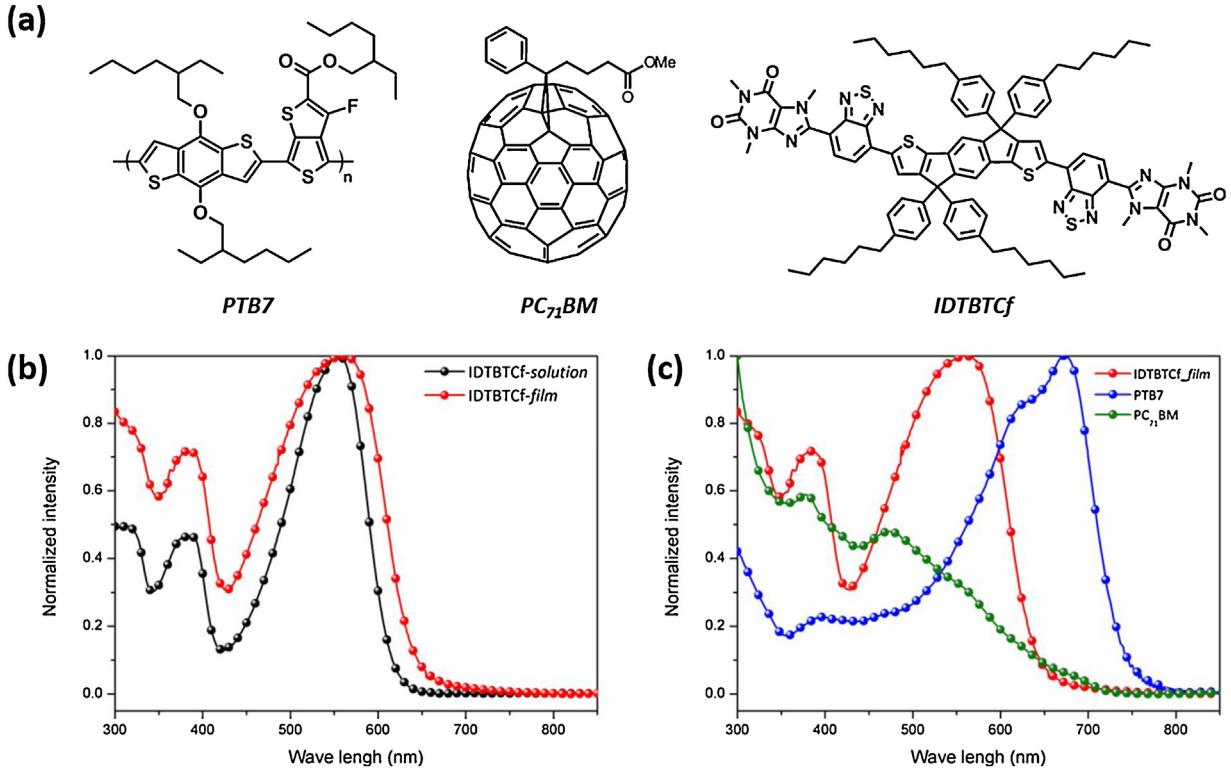

Fig. 2. (a) Chemical structures of active materials (PTB7, $PC_{71}BM$) with IDTBTCf, (b) UV–visible absorption spectra of IDTBTCf in chloroform solution and thin film, (c) UV–visible absorption spectra of active materials with IDTBTCf in thin films.

($E_{1/2}$(ferrocene) = 0.53) was used as the standard material. The LUMO energy level was calculated to be −3.50 eV using the difference between optical band gap value and HOMO energy level. Therefore, it was expected that IDTBTCf has an efficient charge carrier transport characteristic by forming cascade energy levels between PTB7 and $PC_{71}BM$. Measured optical and electrochemical properties of materials were summarized in Table 1.

Photovoltaic properties

Fig. 3(a) and (b) depicted an inverted device structure (ITO/ZnO/active layer/MoO_3/Ag) and energy band diagrams of active layer materials in the inverted structure. The active layer was introduced using spin-coating by dissolving PTB7, $PC_{71}BM$, and small amounts of IDTBTCf in solution. It was confirmed that the energy band diagram of IDTBTCf was located between energy band gap of PTB7 and $PC_{71}BM$, forms cascade-like energy levels well as seen in Fig. 3(b). Such a structure accelerates electric charge transfer at the interfaces between PTB7 and $PC_{71}BM$, and also can accelerate exciton dissociation by connecting energy offset [35,40–42]. Therefore, charge carriers can be expected to move smoothly in PTB7 and $PC_{71}BM$ blend with adding IDTBTCf and also contribute to improving the performance of PSCs.

Table 2 and Fig. 4(a, b) show photovoltaic results depending on the amount of IDTBTCf that was added to the active layer. UV–vis absorption and photoluminescence (PL) spectra at this time are shown in Fig. 4(c) and (d), respectively. As seen in Table 2, V_{OC} was consistent, but J_{SC} and FF slightly increased, resulting in the increase of PCE when IDTBTCf was added. However, it was reduced when more than 5 wt% IDTBTCf was added due to their too high aggregation. This matches well to the results of J–V curve, corresponding external quantum efficiency response (EQE response) and UV–vis spectra in Fig. 4(a–c).

All devices showed a broad response at 300–700 nm, 30–50% values at 350–430 nm, 50–60% values at 430–700 nm on the EQE curve in Fig. 4(b). Other trends were observed high absorption properties at 500–650 nm depending on the addition of IDTBTCf. Thus, high EQE values were obtained in long wavelength (450–700 nm) with 2.5 wt% IDTBTCf. In the PSCs with 5.0 wt% IDTBTCf, low J_{SC} were obtained because the EQE response was lowered than that of the reference in a whole absorption region.

According to Fig. 4(c), the absorption rate of the 500–650 nm area in the absorption wavelength region of IDTBTCf increased in UV absorption spectra of all blend solutions. As more IDTBTCf was added, there was a benefit for the absorbing region, but the efficiency of PSCs was reduced as seen in J–V data. Fig. 4(d) shows Photoluminescence (PL) spectra of each blends. It is confirmed by PL spectra that added IDTBTCf affects recombination of exciton. Neat PTB7 had maxima PL intensity at 758 nm and had 37% quenching efficiency in $PC_{71}BM$ and blend. As PL intensity is lower, the recombination of the charge is prevented, and thus the charge transport characteristic is effectively obtained, which results in improved J_{SC} [9].

The main factor to determine FF is the recombination of exciton. FF is determined by the competition of transport and recombination of charge carriers that reach the electrode among the generated excitons [43]. A PCE increase caused by a FF rise is due to good distribution of IDTBTCf between donor and acceptor materials and thus IDTBTCf effectively increased the packing density with stacking effect through the non-covalent bond. In addition, when 1.5 wt% IDTBTCf was applied, a similar effect was obtained, but it is not optimized. In the case that 5 wt% IDTBTCf was added to device, lower FF and PCE than those of the reference were recorded because the aggregation of active layer materials was accelerated by excess IDTBTCf, which negatively affects morphology formation.

Also, we fabricated that device of PTB7:IDTBTCf = 1:1 blend investigated to know IDTBTCf effects, it displayed close to 0% of PCE as seen in Fig. S7 and Table. S1. Low FF and J_{SC} mean that most of the electrons and holes made in this PSC do not flow to each electrode but are recombined. This is because hydrophilicity of the IDTBTCf solution by too strong polarization effect induced the phase separation of the active layer and thus resulted in poor morphology.

To evaluate long-term stability of fabricated devices, their stability was measured by storing PSCs in a glove box for 172 h. Results for the long-term stability of FF and PCE with 2.5 wt% IDTBTCf (best efficiency) and without IDTBTCf are depicted in Fig. 5. The self-aggregation characteristics of $PC_{71}BM$ caused phase separation as time goes, and thus PCE decreased due to diminishing life-time of exciton because it becomes distant from the exciton diffusion length [43]. However, in the case of a device with IDTBTCf, FF was maintained at values of 65–70% for 172 h, and it showed better stability (degradation rate of efficiency, 8%) than the reference one (degradation rate of efficiency, 15.5%). The addition of IDTBTCf inhibited the migration of both materials by non-covalent interaction force such as Van der Waals forces interaction, hydrogen bonding, and etc., which resulted in maintenance FF and excellent long-term stability of PCE. Thus, IDTBTCf can prevent the decrease of FF due to self-aggregation of $PC_{71}BM$.

To deeply examine the effect of introducing IDTBTCf, we measured the light stability of fabricated devices with encapsulation under the continuous illumination (AM 1.5 G, 100 mW/cm^2) for 4 h in Fig. S8. After 1 h, the PCE of the device without IDTBTCf is dramatically decreased with 4.7% compared to its initial PCE (8.4%), whereas the case by introducing 2.5 wt% IDTBTCf is relatively maintained with 5.1% of PCE (initial PCE, 8.7%), it caused by burn-in-loss phenomenon of the fullerene-based devices. PCEs of both devices are dropped over than a half after 4 h. In the part of light stability, we did not see surprising effect by introducing IDTBTCf in active layer.

Table 1
Optical and electrochemical propertiesof active materials (PTB7, $PC_{71}BM$) with IDTBTCf.

	λ^{Film}_{max} (nm)	λ_{onset} (nm)	$E_g{}^{opt}{}_{onset}$[a] (eV)	HOMO[b] (eV)	LUMO[d] (eV)	T_d[e] (°C)
IDTBTCf	382, 559	640	1.94	−5.44	−3.50	434
PTB7[f]	674	737	1.68	−5.15	−3.47	325
$PC_{71}BM$[g]	377, 473	653	1.90	−5.80	−3.90	425

[c] $E_{1/2}$(Fc/Fc^+ vs Ag/AgCl) = 0.53 eV (measured data).
[a] Calculated from the intersection of the tangent on the low energetic edge of the absorption spectrum with the baseline.
[b] $E_{HOMO\ (or\ LUMO)} = -[E_{onset}$(vs Ag/AgCl) − $E_{1/2}$(Fc/Fc^+ vs Ag/AgCl)[c]] − 4.8eV.
[d] $E_{LUMO} = E_{HOMO} + E_g{}^{opt}$.
[e] A temperature, at which sample shows 5% weight loss under nitrogen gas.
[f] See references [36,37].
[g] See references [37,38].

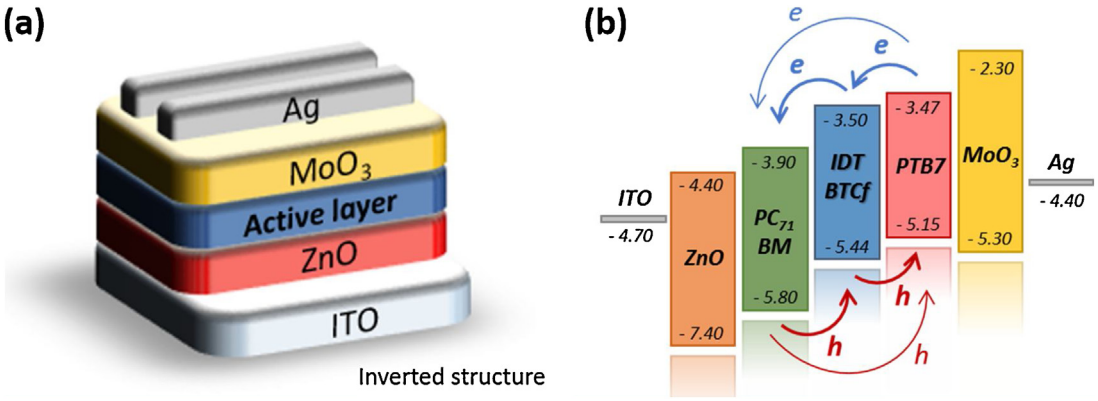

Fig. 3. (a) Inverted structure for PSCs in this study, (b) energy band diagrams of active layer materials in inverted structure [36–39].

Table 2
The photovoltaic parameters of PTB7:$PC_{71}BM$ = 1:1.5 with different concentrations of IDTBTCf for PSCs.

IDTBTCf (wt %)	V_{oc} (V)	J_{sc} (mA/cm^2)	FF (%)	PCE (%)	
				Best	Average
0	0.757	16.2	68.6	8.4	8.1
1.5	0.757	16.3	69.3	8.6	8.2
2.5	0.757	16.3	70.6	8.7	8.3
5	0.757	15.9	65.5	7.9	7.5

Charge carrier transport properties

The mobility of electron and hole of both PTB7:$PC_{71}BM$ = 1:1.5 (reference) device and each device with IDTBTCf (a mass ratio of 1.5 wt%, 2.5 wt%, 5.0 wt% with PTB7) were measured using the space charge limited current (SCLC) method. Each mobility was calculated using the Mott–Gurney space charge limited current formula (Formula (1)). Fig. 6 shows the mobility graph for electrons and holes measured by electron-only devices and hole-only devices, which were fabricated (μ = stands for charge

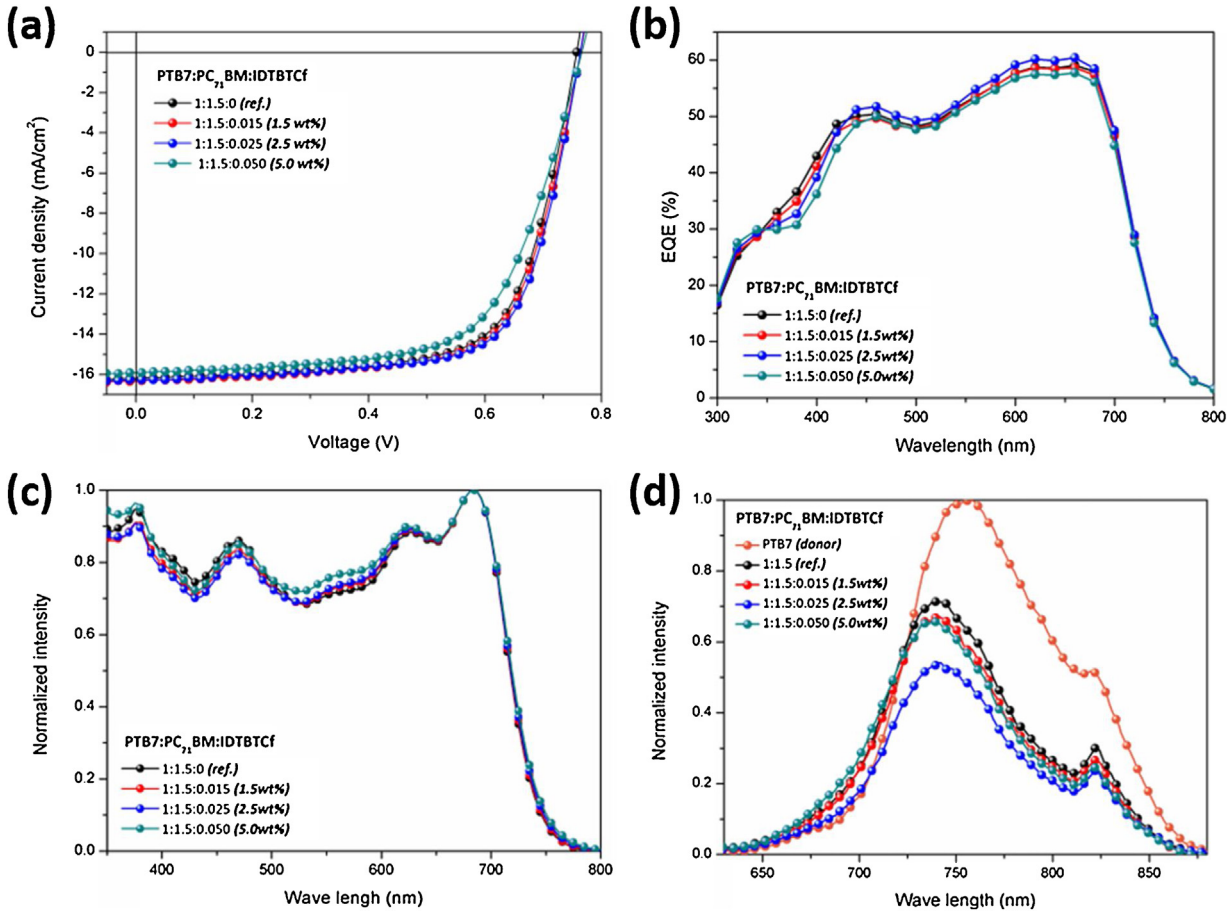

Fig. 4. (a) J–V and (b) EQE curves, (c) UV–visible absorption and (d) PL spectra of PTB7:$PC_{71}BM$ = 1:1.5 with different concentrations of IDTBTCf in thin films for inverted PSCs.

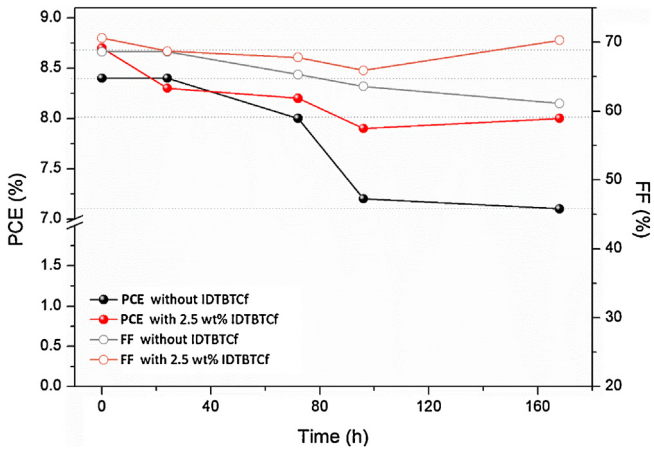

Fig. 5. The results of long-term stability for PSCs.

carrier mobility, ε_0 = the dielectric constant of free-space, ε_r = the permittivity of the active layer, V = the applied voltage, L = thickness of semiconductor layer):

$$J = \left(\frac{9}{8}\right)\mu\varepsilon_0\varepsilon_r\left(\frac{V^2}{L^3}\right) \quad (1)$$

The electron-only device was fabricated as an ITO/ZnO/active layer/LiF/Al structure and the hole-only device was produced as an ITO/PEDOT:PSS/active layer/MoO_3/Ag structure. Electron mobility appeared to be $2.40 \times e^{-04}$ in the reference device and appeared to be 2.42, 2.61 and $2.39 \times e^{-04}$, respectively in devices with IDTBTCf of 1.5, 2.5, and 5.0 wt%, respectively. The mobility of the hole-only device was $2.54 \times e^{-04}$ in the reference device and appeared to be 3.24, 5.25 and $3.01 \times e^{-04}$, respectively, in the device with IDTBTCf. This result showed the same tendency as FF of devices with IDTBTCf.

Film characterization

Contact angle measurements of the reference and blend solutions with various IDTBTCf concentrations are shown in Fig. 7. As seen in Fig. 7(a–d), the contact angle of 103.5° with the reference solution gradually decreased as IDTBTC was more added. As a result, it became 95.3° due to too high hydrophilicity in 5 wt%. solution The addition of adequate amounts of polar materials act as a support in the thin film and can evenly distribute donor and acceptor [26]. The highest FF was obtained in the devices with 2.5 wt% IDTBTCf having the contact angle of 96.1° by evenly dispersing PTB7 and $PC_{71}BM$, which also improved transport of charge carriers.

Tapping mode atomic microscopy (AFM) analysis was performed to compare phase-separated morphologies of PTB7:$PC_{71}BM$ blend films with various IDTBTCf concentrations in Fig. 8. In general, when analyzing images of polymer:$PC_{71}BM$ blend, white parts are interpreted as the dominant distribution of polymer, dark domains are interpreted as aggregations of $PC_{71}BM$ [44]. According to Fig. 8(a–d), white and dark parts indicate PTB7 and $PC_{71}BM$, respectively. The interpenetrating feature with bi-continuous network showed with a small domain size of $PC_{71}BM$ in all films, and there is no big difference in size. When Fig. 8(a) with (c) are compared, however, the image of the reference film was centered in the dark domain by self-aggregation of $PC_{71}BM$, but the white and dark domains tend to be distributed widely and evenly in the image of the film with 2.5 wt% IDTBTCf. This fine morphology improves the transfer of charge carriers between PTB7 and $PC_{71}BM$, and prevents recombination of exciton, and thus J_{SC} and FF were improved.

As seen in Fig. 8(b) and (d), the use of a small amount of 1.5 wt% IDTBTCf showed generally better spreading effect of polymer compared to the reference, but the aggregation of $PC_{71}BM$ domain was shown at the center due to insufficient phase separation. And the film with too much IDTBTCf (5.0 wt %) showed the most aggregation among all films and exerted an adverse effect on the device which is consistent with the result of the decrease of FF and J_{SC}. Root-mean-square roughness (RMS) roughness values showed similar roughness at 1.77 nm, 1.75 nm, 1.85 nm and 1.94 nm with IDTBTCf concentrations, respectively.

XRD analysis was used to analyze the crystalline nature and molecular orientations of the active layer by the addition of IDTBTCf, and the results are showed in Fig. 9. The Out-of-plane XRD analysis results of films of PTB7 and IDTBTCf in CB solution with 3 vol% DIO, respectively, are depicted in Fig. 9(a). Fig. 9(b) depicts the out-of-plane of film made of a solution which is prepared by adding 2.5 wt% IDTBTCf to PTB7:$PC_{71}BM$ solution in same condition. First, in the out-of-plane data of PTB7, the reflection peak was observed at 22.8°, which is corresponding to a π–π stacking. The distance at this time was 3.89 Å, which was calculated by Bragg's low equation ($\lambda = 2d\sin\theta$, Cu, λ: 1.541871 Å, d: distance). IDTBTCf showed a gentle (100) peak at 4.8° and two (010) peaks at 15.96° and 21.11° in a gentle and broad region. This means π–π stacking of the closer nearby materials due

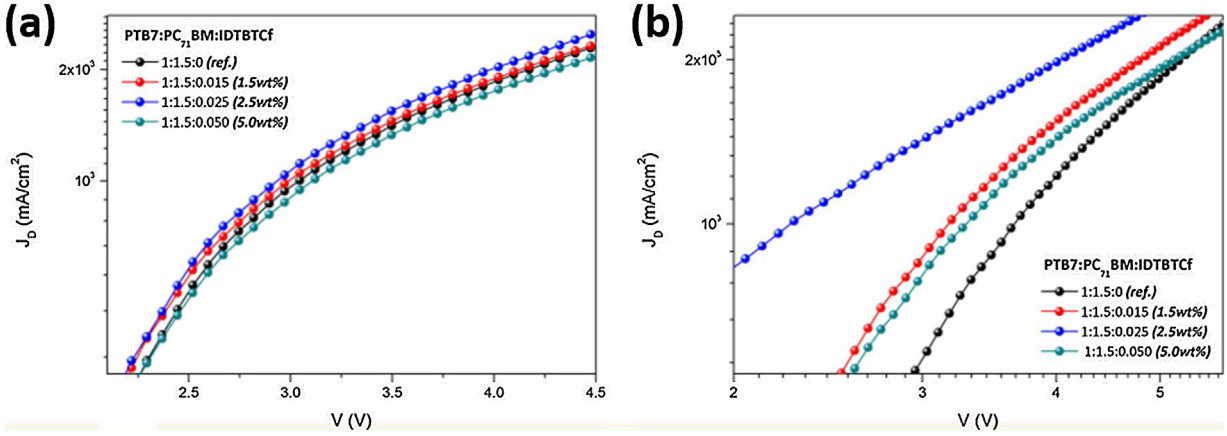

Fig. 6. Charge carrier mobility of PTB7:$PC_{71}BM$ = 1:1.5 with each different concentrations of IDTBTCf for PSCs: (a) electron and (b) hole mobility.

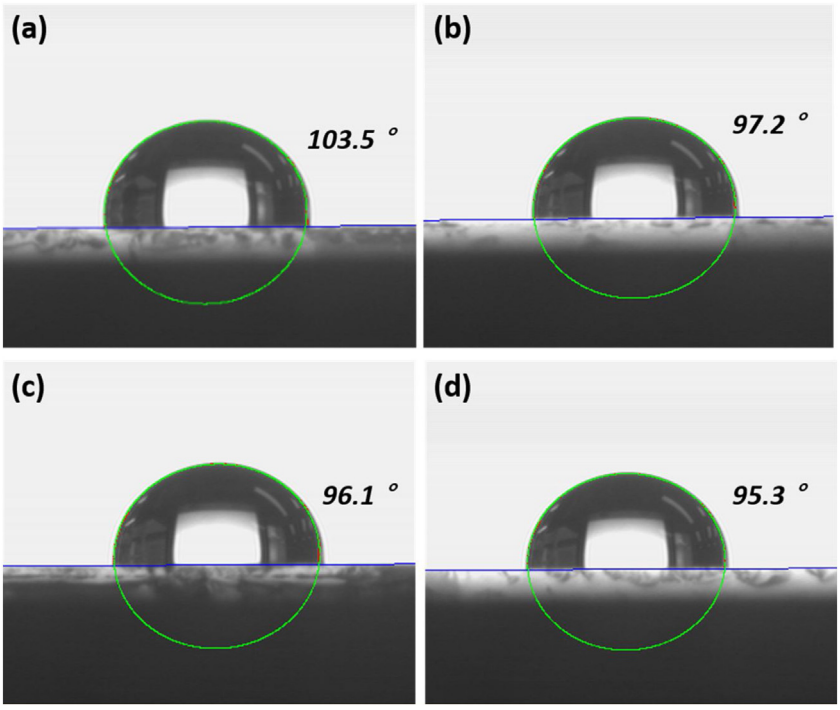

Fig. 7. Contact angle images of (a) PTB7: $PC_{71}BM$ = 1:1.5 and PTB7: $PC_{71}BM$ = 1:1.5 with (b) 1.5 wt%, (c) 2.5 wt% and (d) 5.0 wt% of IDTBTCf.

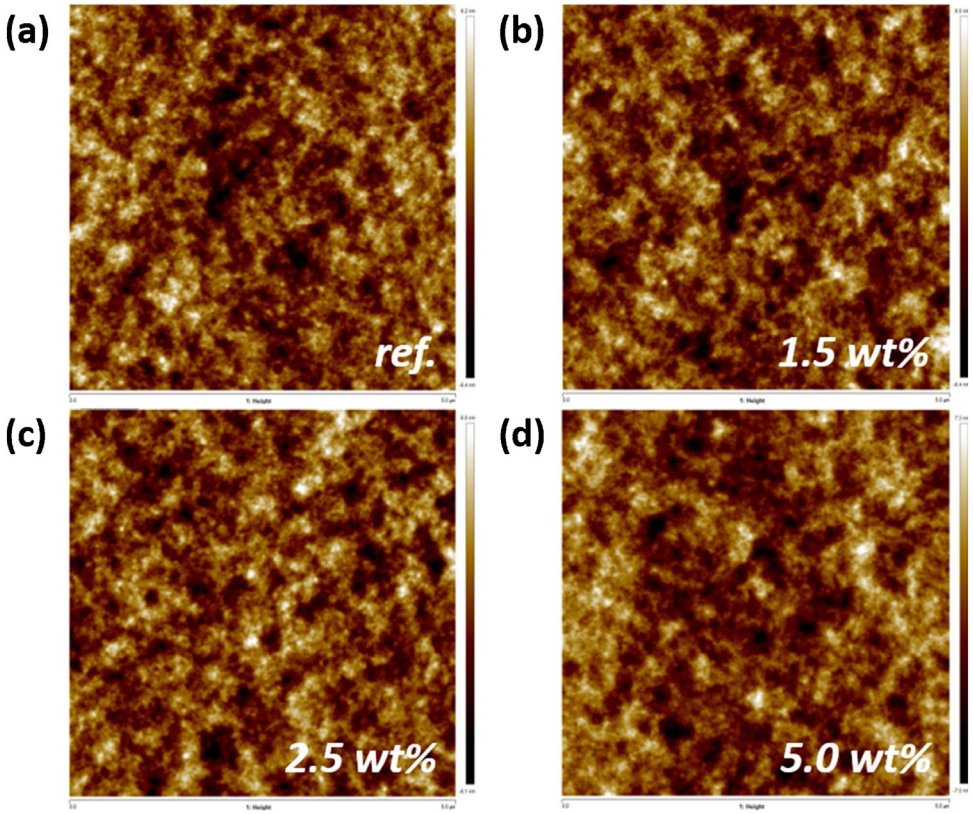

Fig. 8. AFM 2D topography images of PTB7:$PC_{71}BM$ = 1:1.5 with different concentrations of IDTBTCf: (a) without IDTBTCf, (b) with 1.5 wt%, (c) 2.5 wt% and (d) 5.0 wt% of IDTBTCf.

to the planar structure of IDTBTCf and the secondary bonding by non-covalent bonding. Based on the data of PTB7:$PC_{71}BM$, it is observed that a reflection indicating π–π stacking was overlapped with $PC_{71}BM$ peak and indicates a more random orientation [44].

By comparison, in the data of blend with 2.5 wt% IDTBTCf, which is indicated, the intensity of a (100) peak indicating lamella orientation remarkably decreased. There are several peaks at 10.95°, 16.61°, 19.54°, and 25.48° relative to the reference, which

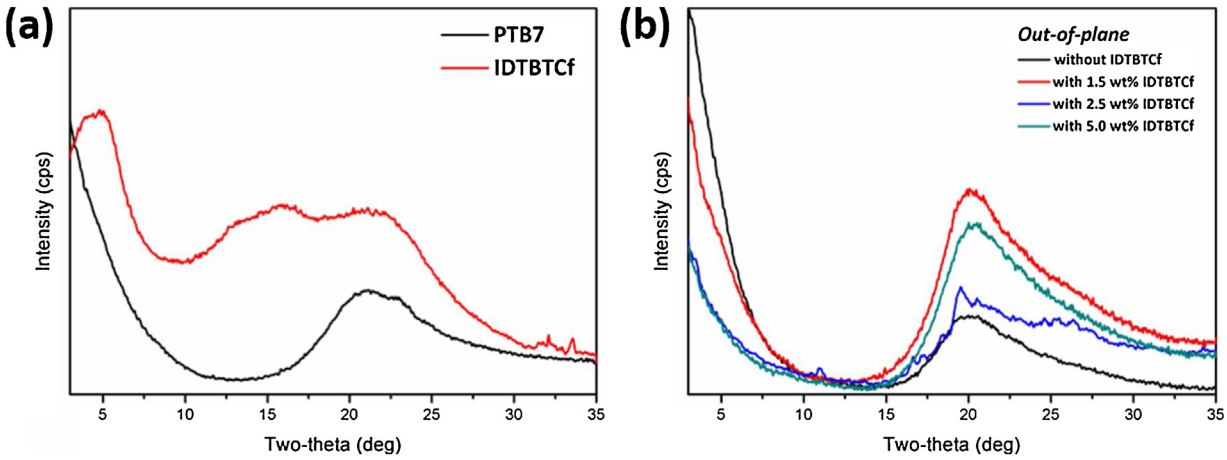

Fig. 9. XRD characteristics for materials in out-of-plane: (a) pristine PTB7 and IDTBTCf films, (b) PTB7:$PC_{71}BM$ = 1:1.5 blend films without/with different concentrations of IDTBTCf.

suggests the addition of IDTBTCf improves the crystallinity of bulk hetero junction blend [45]. In addition, the (010) peak at 25.48° represents π-π stacking reflection of 3.5 Å and is distinct from the $PC_{71}BM$ peak. This suggests that the blend became to have a clearer PTB7 (010) peak and have closer molecular packing due to the addition of IDTBTCf, and preferred more face-on orientation towards the plate. This tendency improves carrier transport [46]. The results of unoptimized concentrations did not show much difference from the reference without ideal stacking changes. As shown in Fig. S9, the results of in-plane data are corresponding to tendency of out-of-plane data.

Conclusion

In this study, we synthesized new small molecule 'IDTBTCf' that has a polar molecule caffeine as an end-group. This was added as the third material of PTB7:$PC_{71}BM$ blend for inverted PSCs. IDTBTCf has an adequate complementary absorption region with PTB7 and $PC_{71}BM$, it formed a cascade energy levels alignment between PTB7 and $PC_{71}BM$ to form more exciton and to improve the transport ability, which in turn inhibits recombination.

The IDTBTCf forms non-covalent interaction in the active layer. Thus, narrows the arrangement and distance of blends, improves π–π stacking by arranging polymer uniformly, and reduces aggregation by preventing $PC_{71}BM$ from self-aggregation via molecular locking of crystallinity of active layer. Based on PSCs properties, a small amount of 2.5 wt% IDTBTCf controlled morphology and improved FF compared to the reference. It resulted in a slightly higher PCE of 8.7% than the reference PCE of 8.4%.

Also, long-term stability measurement without encapsulation in a glove box for 172 h, a device with IDTBTCf (degradation rate of efficiency, 8%) showed better stability than the reference one (degradation rate of efficiency, 15.5%). These works demonstrated that caffeine can be introduced as a new end-group and serve as a good reference to design new materials for polymer solar cells to control morphology.

Acknowledgments

This paper was supported by Konkuk University in 2016.

Appendix A. Supplementary data

Supplementary material related to this article can be found, in the online version, at doi:https://doi.org/10.1016/j.jiec.2019.03.015.

References

[1] A.H. Author, G. Yu, J. Gao, J.C. Hummelen, F. Wudl, A.J. Heeger, Science 270 (5243) (1995) 1789, doi:http://dx.doi.org/10.1126/science.270.5243.1789.
[2] A.J. Heeger, Adv. Mater. 26 (1) (2014) 10, doi:http://dx.doi.org/10.1002/adma.201304373.
[3] C. Liu, K. Wang, X. Gong, A.J. Heeger, Chem. Soc. Rev. 45 (17) (2016) 4825, doi:http://dx.doi.org/10.1039/c5cs00650c.
[4] Y. He, H.-Y. Chen, J. Hou, Y. Li, J. Am. Chem. Soc. 132 (4) (2010) 1377, doi:http://dx.doi.org/10.1021/ja908602j.
[5] W. Zhao, S. Li, H. Yao, S. Zhang, Y. Zhang, B. Yang, J. Hou, J. Am. Chem. Soc. 139 (21) (2017) 7148, doi:http://dx.doi.org/10.1021/jacs.7b02677.
[6] H. Bin, L. Gao, Z.G. Zhang, Y. Yang, Y. Zhang, C. Zhang, S. Chen, L. Xue, C. Yang, M. Xiao, Y. Li, Nat. Commun. 7 (May) (2016) 1, doi:http://dx.doi.org/10.1038/ncomms13651.
[7] Y. Liu, Z. Zhang, S. Feng, M. Li, L. Wu, R. Hou, X. Xu, X. Chen, Z. Bo, J. Am. Chem. Soc. 139 (9) (2017) 3356, doi:http://dx.doi.org/10.1021/jacs.7b00566.
[8] D. Qian, L. Ye, M. Zhang, Y. Liang, L. Li, Y. Huang, X. Guo, S. Zhang, Z. Tan, J. Hou, Macromolecules 45 (24) (2012) 9611, doi:http://dx.doi.org/10.1021/ma301900h.
[9] K. Zhu, D. Tang, K. Zhang, Z. Wang, L. Ding, Y. Liu, L. Yuan, J. Fan, B. Song, Y. Zhou, Y. Li, Org. Electron.: Phys. Mater. Appl. 48 (2017) 179, doi:http://dx.doi.org/10.1016/j.orgel.2017.06.009.
[10] Q. Sun, F. Zhang, J. Hai, J. Yu, H. Huang, F. Teng, W. Tang, Electron. Mater. Lett. 11 (2) (2015) 236, doi:http://dx.doi.org/10.1007/s13391-014-4326-9.
[11] Y.W. Han, S.J. Jeon, J.Y. Choi, J.H. Kim, D.K. Moon, Sol. RRL 1800077 (2018) 1800077, doi:http://dx.doi.org/10.1002/solr.201800077.
[12] L. Dou, J. You, J. Yang, C.C. Chen, Y. He, S. Murase, T. Moriarty, K. Emery, G. Li, Y. Yang, Nat. Photonics 6 (3) (2012) 180, doi:http://dx.doi.org/10.1038/nphoton.2011.356.
[13] T. Jiang, Z. Xue, M. Ford, J. Shaw, X. Cao, Y. Tao, Y. Hu, W. Huang, RSC Adv. 6 (82) (2016) 78720, doi:http://dx.doi.org/10.1039/c6ra14327j.
[14] J. You, L. Dou, K. Yoshimura, T. Kato, K. Ohya, T. Moriarty, K. Emery, C.C. Chen, J. Gao, G. Li, Y. Yang, Nat. Commun. 4 (2013) 1410, doi:http://dx.doi.org/10.1038/ncomms2411.
[15] J. Huang, H. Wang, K. Yan, X. Zhang, H. Chen, C.Z. Li, J. Yu, Adv. Mater. 29 (19) (2017) 1, doi:http://dx.doi.org/10.1002/adma.201606729.
[16] H.H. Gao, Y. Sun, X. Wan, X. Ke, H. Feng, B. Kan, Y. Wang, Y. Zhang, C. Li, Y. Chen, Adv. Sci. (2018) 1, doi:http://dx.doi.org/10.1002/advs.201800307 1800307.
[17] W. Zhong, J. Cui, B. Fan, L. Ying, Y. Wang, X. Wang, G. Zhang, X.F. Jiang, F. Huang, Y. Cao, Chem. Mater. 29 (19) (2017) 8177, doi:http://dx.doi.org/10.1021/acs.chemmater.7b02228.
[18] H.J. Son, B. Carsten, I.H. Jung, L. Yu, Energy Environ. Sci. 5 (8) (2012) 8158, doi:http://dx.doi.org/10.1039/c2ee21608f.
[19] Q. An, F. Zhang, Q. Sun, J. Wang, L. Li, J. Zhang, W. Tang, Z. Deng, J. Mater. Chem. A 3 (32) (2015) 16653, doi:http://dx.doi.org/10.1039/c5ta04243g.
[20] Z. Luo, W. Xiong, T. Liu, W. Cheng, K. Wu, Y. Sun, C. Yang, Org. Electron.: Phys. Mater. Appl. 41 (2017) 166, doi:http://dx.doi.org/10.1016/j.orgel.2016.10.044.
[21] M.A. Uddin, H.Y. Woo, M.J. Cho, D.H. Choi, ACS Appl. Mater. Interfaces 9 (10) (2017) 8838–8847, doi:http://dx.doi.org/10.1021/acsami.6b15707.
[22] Z. Zhang, L. Feng, S. Xu, Y. Liu, H. Peng, Z.G. Zhang, Y. Li, Y. Zou, Adv. Sci. 4 (11) (2017) 1, doi:http://dx.doi.org/10.1002/advs.201700152.
[23] B. Zhao, W. Wang, J. Xin, H. Wu, H. Liu, Z. Guo, Z. Cong, W. Ma, C. Gao, ACS Sustain. Chem. Eng. 6 (2) (2018) 2177, doi:http://dx.doi.org/10.1021/acssuschemeng.7b03606.
[24] Y. Lin, X. Zhan, Acc. Chem. Res. 49 (2) (2016) 175, doi:http://dx.doi.org/10.1021/acs.accounts.5b00363.
[25] F. Zhao, S. Dai, Y. Wu, Q. Zhang, J. Wang, L. Jiang, Q. Ling, Z. Wei, W. Ma, W. You, C. Wang, X. Zhan, Adv. Mater. 29 (18) (2017) 1, doi:http://dx.doi.org/10.1002/adma.201700144.
[26] P. Cheng, C. Yan, T.K. Lau, J. Mai, X. Lu, X. Zhan, Adv. Mater. 2 (2016) 5822, doi:http://dx.doi.org/10.1002/adma.201600426.

[27] X. Song, M. Fan, K. Zhang, D. Ding, W. Chen, Y. Li, L. Yu, M. Sun, R. Yang, Macromol. Rapid Commun. 39 (8) (2018) 1, doi:http://dx.doi.org/10.1002/marc.201700782.
[28] S. Marchetti, An Interdisciplinary Investigation into Alcohol, Caffeine, and Prozac, McMaster University – Honours Integrated Science I, 2016.
[29] X. Wang, K. Wang, M. Wang, Polym. Chem. 6 (10) (2015) 1846, doi:http://dx.doi.org/10.1039/C4PY01627K.
[30] H. Hu, K. Jiang, G. Yang, J. Liu, Z. Li, H. Lin, Y. Liu, J. Zhao, J. Zhang, F. Huang, Y. Qu, H. Yan, J. Am. Chem. Soc. 137 (44) (2015) 14149–14157, doi:http://dx.doi.org/10.1021/jacs.5b08556.
[31] J. Wang, S. Wang, C. Duan, F.J.M. Colberts, J. Mai, X. Liu, X. Jia, X. Lu, R.A.J. Janssen, F. Huang, Y. Cao, Adv. Energy Mater. 7 (22) (2017), doi:http://dx.doi.org/10.1002/aenm.201702033.
[32] J. Lee, J.H. Kim, B. Moon, H.G. Kim, M. Kim, J. Shin, H. Hwang, K. Cho, Macromolecules 48 (6) (2015) 1723, doi:http://dx.doi.org/10.1021/acs.macromol.5b00056.
[33] Y. Li, L. Zhong, F.-P. Wu, Y. Yuan, H.-J. Bin, Z.-Q. Jiang, Z. Zhang, Z.-G. Zhang, Y. Li, L.-S. Liao, Energy Environ. Sci. 9 (11) (2016) 3429, doi:http://dx.doi.org/10.1039/C6EE00315J.
[34] W. Su, Q. Fan, X. Guo, J. Chen, Y. Wang, X. Wang, P. Dai, C. Ye, X. Bao, W. Ma, M. Zhang, Y. Li, J. Mater. Chem. A 6 (17) (2018) 7988, doi:http://dx.doi.org/10.1039/c8ta01509k.
[35] T. Ameri, P. Khoram, J. Min, C.J. Brabec, Adv. Mater. 25 (31) (2013) 4245, doi:http://dx.doi.org/10.1002/adma.201300623.
[36] Y. Liang, Z. Xu, J. Xia, S.T. Tsai, Y. Wu, G. Li, C. Ray, L. Yu, Adv. Mater. 22 (20) (2010) 135, doi:http://dx.doi.org/10.1002/adma.200903528.
[37] L. Fernandes, H. Gaspar, J.P.C. Tomé, F. Figueira, G. Bernardo, Polym. Bull. 75 (2) (2018) 515, doi:http://dx.doi.org/10.1007/s00289-017-2045-8.
[38] F. Zhang, Z. Zhuo, J. Zhang, X. Wang, X. Xu, Z. Wang, Y. Xin, J. Wang, J. Wang, W. Tang, Z. Xu, Y. Wang, Sol. Energy Mater. Sol. Cells 97 (2012) 71, doi:http://dx.doi.org/10.1016/j.solmat.2011.09.006.
[39] Q. Zhang, R. Peng, C. Zhang, D. Chen, Z. Lin, J. Chang, J. Zhang, Y. Hao, Polymers (Basel) 10 (2) (2018), doi:http://dx.doi.org/10.3390/polym10020127.
[40] H. Lu, J. Zhang, J. Chen, Q. Liu, X. Gong, S. Feng, X. Xu, W. Ma, Z. Bo, Adv. Mater. 28 (43) (2016) 9559, doi:http://dx.doi.org/10.1002/adma.201603588.
[41] M. Koppe, H.-J. Egelhaaf, G. Dennler, M.C. Scharber, C.J. Brabec, P. Schilinsky, C. N. Hoth, Adv. Funct. Mater. 20 (2) (2010) 338, doi:http://dx.doi.org/10.1002/adfm.200901473.
[42] M. Koppe, H.J. Egelhaaf, E. Clodic, M. Morana, L. Lüer, A. Troeger, V. Sgobba, D.M. Guldi, T. Ameri, C.J. Brabec, Adv. Energy Mater. 3 (7) (2013) 949, doi:http://dx.doi.org/10.1002/aenm.201201076.
[43] S. Günes, H. Neugebauer, N.S. Sariciftci, Chem. Rev. 107 (4) (2007) 1324, doi:http://dx.doi.org/10.1021/cr050149z.
[44] F. Liu, W. Zhao, J.R. Tumbleston, C. Wang, Y. Gu, D. Wang, A.L. Briseno, H. Ade, T. P. Russell, Adv. Energy Mater. 4 (5) (2014) 1, doi:http://dx.doi.org/10.1002/aenm.201301377.
[45] Y. Zheng, J. Huang, G. Wang, J. Kong, D. Huang, M. Mohadjer Beromi, N. Hazari, A.D. Taylor, J. Yu, Mater. Today 21 (1) (2018) 79, doi:http://dx.doi.org/10.1016/j.mattod.2017.10.003.
[46] N.A. Ran, S. Roland, J.A. Love, V. Savikhin, C.J. Takacs, Y.T. Fu, H. Li, V. Coropceanu, X. Liu, J.L. Brédas, G.C. Bazan, M.F. Toney, Di. Neher, T.Q. Nguyen, Nat. Commun. 8 (1) (2017) 1, doi:http://dx.doi.org/10.1038/s41467-017-00107-4.